EFFECT OF GEOMETRICAL HARDENING AND STABILITY ON THE FORMABILITY OF FCC SHEET METALS WITH AN INITIAL 45° ND ROTATED CUBE ORIENTATION IN PLANE-STRAIN STRETCHING

María A. Bertinetti[a], Claudio D. Schwindt[b] and Javier W. Signorelli[a]

[a] *Grupo de Física y Micromecánica de Materiales Heterogéneos, Instituto de Física Rosario, Universidad Nacional de Rosario, Bv. 27 de Febrero 210b, Rosario, Argentina – CONICET, bertinetti@ifir-conicet.gov.ar; signorelli@ifir-conicet.gov.ar*

[b] *Grupo de Metalurgia, Universidad Nacional del Sur, Avenida Alem 1253 - Bahía Blanca(8000FTN), Argentina – CONICET, claudio.schwindt@uns.edu.ar*

Keywords: Crystallographic textures, stability, geometrical hardening, MK-VPSC approach.

Abstract. The stability of ideal orientations is a key aspect in the characterization and understanding of texture evolution during plastic deformation. As is well known, texture evolution, and hence anisotropy, strongly affects formability. In this research, we examine the limit-strain values in the plane-strain stretching mode, in terms of the evolution and stability of crystallographic orientations. The effect that geometric or textural hardening has on the macroscopic response is also quantified.

In particular, we are focusing on the behavior of recrystallized FCC alloy sheets (like aluminum) with initial{100}<100> cube orientations, when the orthotropic axes are inclined at 45 degrees relative to the rolling direction and lying near plain-strain forming paths. As reported in the literature (Lopes et al., 2003; Yoshida et al., 2007, 2009), the limit-strain values are significantly increased near these plane-strain forming paths. In order to understand how these orientations evolve in the Euler space, lattice rotation field maps were calculated using the Full Constraint (FC) and Viscoplastic Self-Consistent (VPSC) models. Results show that these orientations are metastable during rolling and, as deformation proceeds, rotate to Copper and Taylor orientations. The correlation between orientation stability and geometrical hardening is linked to the high formability in plane-strain loading. Texture evolution and the limit-strain predicted by VPSC are in agreement with experimental data reported by Liu and Morris (2002) and Lopes et al. (2003) respectively.

1   INTRODUCTION

Most sheet metals employed in stretch forming operations are produced by a combination of rolling and annealing. As a consequence, typical preferred orientations are inevitably present in rolled sheets that cannot be completely transformed to an entirely random state by annealing. Investigation of the behavior of these orientations contributes to a deeper understanding of material deformation mechanisms, microstructural evolution and mechanical anisotropy. It is widely recognized that crystallographic textures strongly affect the formability of polycrystalline sheet metals. In rolled FCC sheets, crystallographic textures are frequently classified in terms of the ideal rolling and recrystallization components.

Many researchers have investigated, experimentally and computationally, the influence of different starting textures and work-hardening behavior on the deformation of aluminum sheets, including the development of material anisotropy. Among others, Choi et al. (2000) studied the macroscopic anisotropy of AA5019A sheets, containing the typical texture components of the H48 and O temper conditions. The cold-rolled material (AA5019A H48) has a strong rolling texture and weak Cube component, while the AA5019A-O sheet contains a strong cube and minimal rolling texture components. Their experimental investigation included tension tests to measure yield stresses and plastic-strain ratios, and predictions of plastic properties were performed with both Taylor (FC) and viscoplastic self-consistent (VPSC) models. They concluded that the FC model not only underestimated r-values, particularly for loading at 45° to the rolling direction, but incorrectly predicted the orientational dependence of yield stress. To the contrary, the VPSC simulations were in good agreement with the experimental results. Lopes et al. (2003) extensively studied a recrystallized, strongly Cube textured AA1050-O sheet in order to gain insight on how crystallographic texture affects strain-hardening anisotropy in proportional tensile loading. In their research, the authors deformed tensile specimens oriented at 0°, 45° and 90° to the rolling direction (RD), measuring the stress-strain behavior. They observed that the 45° orientation exhibited much higher strain hardening, and as a result, 30 and 25 % greater uniform elongations, respectively, than the 0° and 90° specimens. Similarly, the measured strain-rate sensitivity exponent, m, at 45° was higher than that in the transverse direction. They suggested that post-uniform elongation ductility could be higher for 45° tension, making this direction very resistant to plastic-flow localization. Later, Yoon et al. (2005) investigated the same AA1050-O alloy, confirming a preponderant {100}<001> cube texture in the {111} pole figure for the as-received material. They also observed that the strain hardening was higher at 45° than in the rolling and transverse directions.

Within a computational framework, Wu et al. (2004) analyzed forming limits for a family of cube textures that had some orientations spreading around the ideal {001}<001>. They found, unexpectedly, that the calculated forming-limit diagrams (FLDs) near biaxial stretching are significantly higher for texture dispersions of 11 and 15 degrees around the ideal cube orientation than for a random texture. Yoshida et al. (2007) made the same observation, finding that it is only the Cube-texture component that produces this result. Moreover, they reported that the forming-limit curve for a cube texture is significantly increased when the sheet is stretched along the 45° direction relative to the rolling direction. This effect is pronounced near plane-strain forming paths. Such a result is in agreement with the reported by Yanaga et al. (2012) of a higher hardening exponent at 45° than at 0° and 90° for a high cube 6061-T4 aluminum alloy sheet. Nevertheless, Yoshida and co-workers found that the predicted limit-strain drastically drops in uniaxial stretching for an ideal Cube texture with a Gaussian spread of 15 degrees. Subsequently, Yoshida et al. (2009) showed that the

{001}<uvw> texture enhances the forming limit curve for the full range of linear strain paths. They concluded that, for a general stamping operation, the {001}<uvw> texture is highly advantageous because of its high formability irrespective of the orientation of the blank. However, the authors note that these results are entirely computational, based on the polycrystal-plasticity model. They also acknowledge that both the strain hardening and forming limit of the strong Cube textured and/or rotated Cube textured aluminum alloy sheets have not been observed experimentally. These sheets were numerically subjected to plane strain and equi-biaxial stretching modes. It is important to mention that all calculations performed by Wu and by Yoshida were based on a generalized FC Taylor-type polycrystal model in conjunction with a Marciniak-Kuczynski (2009) instability analysis (MK). Bertinetti et al. (2008) and Signorelli and Bertinetti (2009) revisited the cube-texture results discussed by Wu et al. (2004), but used a VPSC formulation plus the MK approach. The simulations carried out in this framework gave qualitatively different results than the MK-FC approach when limit strains were calculated from the ideal cube orientation through various dispersions to the random texture. A smooth transition in calculated failure strains was predicted using the MK-VPSC approach. Also, these MK-VPSC calculations predicted that a random texture would give the greatest biaxial formability, as expected. These results demonstrate that the constitutive model selected is critical important for predicting the behavior of materials that evolve anisotropically during mechanical deformation.

The present contribution includes initial {100}<100> Cube orientations when the orthotropic axes are inclined at 45 degrees relative to the rolling direction – R-Cube type materials – and stability analysis, which complements our previous work that investigated the role of the constitutive relation in modeling the forming limit of FCC sheet metal with Cube orientations (Bertinetti et al., 2008; Signorelli and Bertinetti, 2009). The current objective is to examine the particular behavior of the limit-strain curves, especially near the plane-strain stretching mode. First, the predicted FLDs for the two Cube-type textures are evaluated. Because it is known that the Cube and R-Cube orientations are not stable for particular applications, this theoretical study was performed using an orientation stability analysis. Finally, we discuss the geometrical hardening / softening effects predicted by the FC and VPSC models and how they affect the limit-strain behavior. Results show that, in the plane-strain mode, the observed limit-strain behavior is in agreement with the predicted geometrical hardening.

2 SHEET NECKING ANALYSIS

2.1 Constitutive model

To simulate the material response, fully accounting for its heterogeneity and anisotropy, a rate-dependent polycrystalline model is employed. The model starts from the viscoplastic behavior of single crystal and uses a self-consistent homogenization scheme for the transition to polycrystal response. The VPSC formulation to model the aggregate behavior is implemented in conjunction with the well-known MK approach. As it has been originally proposed by Marciniak and Kuczynski, their analysis postulated the existence of a material imperfection such as a groove or a narrow band across the width of the sheet.

A detailed discussion of the integration of the polycrystalline model can be found either in a previous edition of the ENIEF congress (Schwindt et al., 2012) or in the literature (Serenelli et al., 2011; Signorelli et al., 2012).

2.2 Forming limit diagrams for the Cube and R-Cube orientations

For the purpose of investigating how the typical recrystallization textures affect formability, we selected two textures that were observed in aluminum sheets after certain deformation processes. These textures were modeled by spreading the grain orientations around the ideal cube component {100}<001> and the ideal {100}<001> rotated 45° with respect to the orthotropic axes, or {100}<011>. For convenience, the {100}<011> orientation is referred as the R-Cube orientation. These discrete orientations were reoriented in such a way that a Gaussian distribution results. The procedure for generating textures is the same as used in previous work (Signorelli and Bertinetti, 2009). For example, the "Cube texture" is one whose grains have a misorientation with respect to the ideal cube orientation {100}<001> of less than 15 degrees, but only 2/3 of its orientations are within 15 degrees of the ideal orientation. The number of individual orientations was set in order to obtain an adequate representation of the orthotropic symmetries of a rolled sheet. Figure 1 shows the {111} stereographic pole figures for the Cube and R-Cube distributions, where 1500 discretized orientations were used to create the set of textures.

Cube   R-Cube
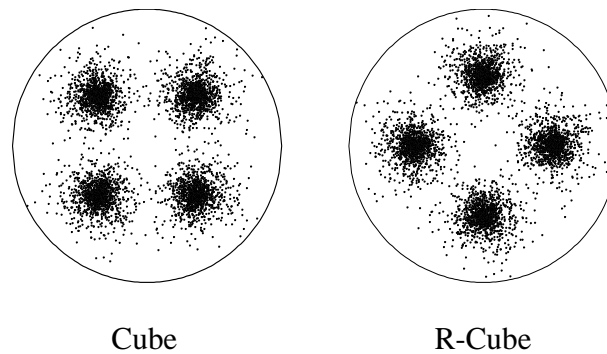
Figure 1: Generated {111} pole figures with 1500 orientations. Gaussian distribution with a standard deviation of 15 degrees.

In the following FLD simulations, in both the homogeneous zone and defect band, standard FCC {111}<110> crystallographic slip is used, and the initial textures are assumed to be the same. The material parameters are taken from Signorelli and Bertinetti (2009), and are fixed as $m = 0.02$, $n = 0.24$, $h_0 = 1218$MPa and $\tau_0 = 42$MPa. The slip-induced hardening law is isotropic for all slip systems, and the reference plastic shearing rate for slip is $\dot{\gamma}_0 = 0.001$ s^{-1}. We took the initial ratio of the thickness inside the band to that outside the band, f_0, to be 0.99 for all computations. Figure 2 shows the predicted FLDs for the set of texture distributions using both MK-FC and MK-VPSC models. Results are similar but not equal to those reported by Yoshida et al. (2007, 2009) when the MK-FC approach is used. Differences appear due to the different parameter values employed in our simulations (curves are identical when calculations are carried out with the set of parameters employed by these authors). The results clearly illustrate the differences between both homogenization schemes, particularly in tensile and biaxial stretching, although the tendency is close for the plane-strain mode ($\rho = 0$). In negative strain space ($\rho < 0$) both models predict similar shapes and levels for the Cube set of orientations. The behavior is quite different for the R-Cube texture, since the FC's predicted curve slopes downwards from plane-strain to a tensile stretching state with the minimum limit-strain value at $\rho = -0.5$. These values are far below than those calculated for the Cube texture. This loss of formability, also predicted by Yoshida et al. (2009), does not appear when the MK-VPSC scheme is used. To the contrary, the R-Cube texture exhibits an

enhanced formability, and the limit-strain values are still higher than those determined from the other texture. For the plane-strain mode, no significant differences are found between approaches, though the VPSC overestimates the limit-strain values for the R-Cube, producing a limit strain 1.4 times greater than that calculate with the FC model. On the biaxial side of the FLD, shapes and values are quite different. As we move towards balanced-biaxial loading, the FLDs approach each other and a certain matching is observed for the two textures, particularly for the VPSC calculations.
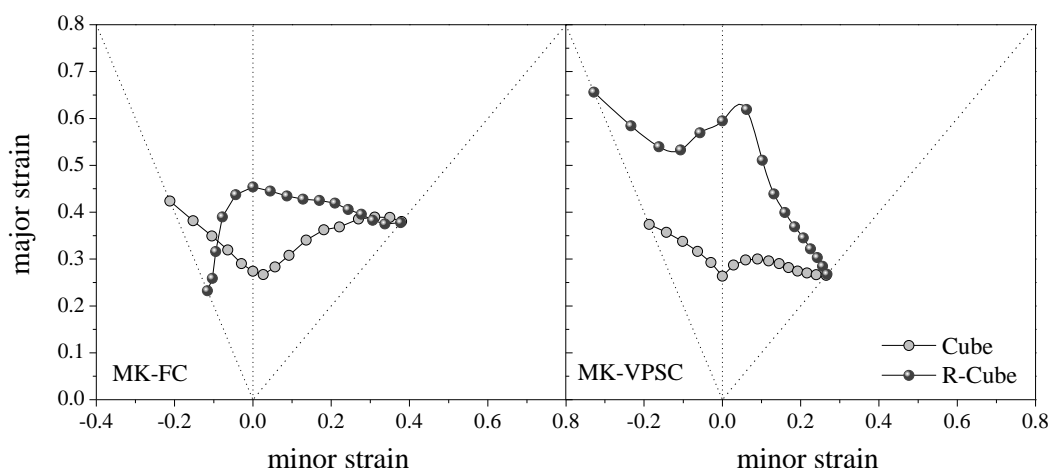
Figure 2: Calculated FLDs assuming a Gaussian distribution with a standard deviation of 15 degrees.

Several authors (Lopes et al., 2003; Yoon et al., 2005; Yoshida et al., 2009) had observed enhanced formability for strong Cube textured aluminum sheets, when they were subjected to uniaxial tension at 45 degrees to the rolling direction. However, there is still not enough experimental limit-strain and strain-hardening data available for R-Cube textured material for us to verify the models' calibration and predictions in plane strain and equi-biaxial stretching modes.

3   STABILITY AND ROTATION FIELDS ANALYSIS

In this section, we follow the work of Tóth et al. (1989) to provide a short description of the basic tenets of orientation stability analysis. Each orientation is defined in the Euler space by three angles $\varphi_1, \phi, \varphi_2$. Texture evolution means that orientations move during plastic deformation in the orientation space, and the orientation change of a given grain can be described, as shown in Clement and Coulomb (1979), by the rotation field:

$$
\begin{aligned}
\dot{\varphi}_1 &= \dot{\Omega}_{21} - \dot{\varphi}_2 \cos\phi \\
\dot{\phi} &= \dot{\Omega}_{32} \cos\varphi_1 + \dot{\Omega}_{13} \sin\varphi_1 \\
\dot{\varphi}_2 &= \left(\dot{\Omega}_{23}\sin\varphi_1 - \dot{\Omega}_{13}\cos\varphi_1\right)/\sin\phi
\end{aligned}
\tag{1}
$$

where $\dot{\Omega}$ is the lattice rotation rate.

One of the conditions for either convergence or divergence of a given orientation can be expressed by the divergence of the rotation field $\dot{\varphi}_1, \dot{\phi}, \dot{\varphi}_2$:

$$
div = \frac{\partial \dot{\varphi}_1}{\partial \varphi_1} + \frac{\partial \dot{\phi}}{\partial \phi} + \frac{\partial \dot{\varphi}_2}{\partial \varphi_2}.
\tag{2}
$$

The condition $div < 0$ and $div > 0$ indicates convergence or divergence, respectively. An orientation can remain stable only if the lattice-rotation rate vanishes and the rotation field in

Euler space is such that it converges on that point. A second parameter related to the stability of an orientation can be examined through the persistence value, P, given by:

$$P(\dot{\varphi}_1, \dot{\phi}, \dot{\varphi}_2, D_{eq}) = \ln\left(\frac{D_{eq}}{\dot{\varphi}_1^2 + \dot{\phi}^2 + \dot{\varphi}_2^2 + 2\dot{\varphi}_1\dot{\varphi}_2\cos\phi}\right) = \ln\left(\frac{D_{eq}}{\|\dot{\Omega}\|}\right) \tag{3}$$

where D_{eq} is the von Mises equivalent strain-rate. The dependency of P on $\cos\phi$ is a direct consequence of the non-Euclidian metric of the Euler space (Beausir et al., 2007). The application of this expression is not valid for all the range of angles, since this parameter can be infinity when $\dot{\varphi}_1, \dot{\phi}, \dot{\varphi}_2$ are null or, equivalently, when $\dot{\Omega} = 0$. Arzaghi et al. (2009) overcome this difficulty proposing a sort of normalization of the lattice spin in the whole Euler space using the maximum value of $\|\dot{\Omega}\|$. Later, Pandey et al. (2012) modified the stability parameter as follows:

$$P = \ln\left(\frac{D_{eq}}{\|\dot{\Omega}\| + D_{eq}/e^{Pmax}}\right). \tag{4}$$

The value $P_{max} = 1$ in Eq. (4) was selected so that P can vary between 0 and 1. The advantages of this equation is that it can never lead to singularities.

3.1 Stability and rotation fields around Cube and R-Cube orientations

To examine the stability of the ideal Cube and R-Cube orientations, during plane-strain, the rotation rates, their gradients and divergences were calculated using the FC and the VPSC schemes. In the last case, a Gaussian distribution of 15 degrees was assumed as Homogeneous effective medium. The degeneracy which arises at $\phi = 0°$ is avoided by taking one of the symmetric equivalents of the Cube and R-Cube orientations defined by the Euler angles $\varphi_1 = 0°$, $\phi = 90°$, $\varphi_2 = 90°$ and $\varphi_1 = 45°$, $\phi = 90°$, $\varphi_2 = 90°$, respectively. The quantities that involve a derivative with respect to the angular values were evaluated through finite differences in the Euler space. The full characteristics of the rotation field around a given orientation were calculated in the initial state as well as at the end of the simulation just before reaching the limit-strain. Numerical results are presented in Table 1 and Table 2, for Cube and R-Cube respectively.

The calculated values for the ideal Cube orientation in plane-strain, at an initial state of deformation, were verified with those reported by Zhou and Neale (1994). It is seen from Table 1 that there is no change of the rotation rates ($\dot{\varphi}_1, \dot{\varphi}, \dot{\varphi}_2$) during plane-strain stretching for the FC case; one of the three terms in the divergence expression is positive, one is zero and the other is negative. This implies that, during plane-strain, orientations rotate towards the cube along the direction of the φ_1 axis, but move away along the φ axis. Under the VPSC scheme the same tendency is observed, but the calculated values for the gradients are much larger than those of FC, implying that the rotation from the ideal Cube orientation will be faster than the FC's predictions, which is consistent with the simulated evolution texture obtained for each model. Based on the rotation rates and the gradients values presented in Table 2, FC predicts that R-Cube is metastable in plane-strain condition. VPSC's calculations show this type of behavior only at the beginning of the deformation, and the difference between both models is given by the magnitude of the divergence terms. Values for the VPSC model are nearly three times greater than those for FC's. Close to the failure strain, the VPSC's values show that the initial R-Cube orientation becomes more stable as it approaches the ideal Taylor orientation during the plane-strain state.

	FC		VPSC	
	initial	close to failure	initial	close to failure
φ_1	0.00	0.00	0.00	-0.02
ϕ	90.00	90.00	90.00	89.89
φ_2	90.00	90.00	90.00	90.00
$\dot{\varphi}_1$	0.00	0.00	0.00	0.00
$\dot{\phi}$	0.00	0.00	0.00	-0.01
$\dot{\varphi}_2$	0.00	0.00	0.00	0.00
$\partial\dot{\varphi}_1/\partial\varphi_1$	-1.00	-1.00	-2.53	-3.31
$\partial\dot{\phi}/\partial\phi$	1.00	1.00	2.41	2.84
$\partial\dot{\varphi}_2/\partial\varphi_2$	0.00	0.00	0.00	-1.10
$div\ \dot{g}$	0.00	0.00	-0.12	-1.57
P	1.00	0.93	0.86	0.79

Table 1: Orientation rate, gradient, divergence and persistence of the ideal Cube orientation in plane-strain (L_{11}=1, L_{22}=0, L_{33}=-1) loading calculated with the FC and VPSC models.

	FC		VPSC	
	initial	close to failure	initial	close to failure
φ_1	45.00	44.92	45.00	41.46*
ϕ	90.00	90.00	90.00	70.04
φ_2	90.00	90.00	90.00	111.13
$\dot{\varphi}_1$	0.00	-0.01	0.00	-0.18
$\dot{\phi}$	0.00	0.00	-0.01	-0.41
$\dot{\varphi}_2$	0.00	0.00	0.01	0.51
$\partial\dot{\varphi}_1/\partial\varphi_1$	1.00	1.00	3.49	1.83
$\partial\dot{\phi}/\partial\phi$	2.50	2.49	7.02	-5.86
$\partial\dot{\varphi}_2/\partial\varphi_2$	2.49	2.51	7.02	-6.31
$div\ \dot{g}$	5.99	5.99	17.53	-10.34
P	0.84	0.75	0.76	0.35

* The misorientation between (φ_1=41.46°, ϕ=70.04°, φ_2=111.13°) and the ideal Taylor (φ_1=90.00°, ϕ=27.00°, φ_2=45.00°) is 1.37 degrees.

Table 2: Orientation rate, gradient, divergence and persistence of the ideal R-Cube orientation in plane-strain (L_{11}=1, L_{22}=0, L_{33}=-1) loading calculated with the FC and VPSC models.

In order to visualize how an individual orientation in the vicinity of the ideal one evolves in the Euler space, typical cross-sections of the rotation field: $\phi - \varphi_1$, $\varphi_2 - \varphi_1$, and $\varphi_2 - \phi$, were plotted to illustrate the reorientation tendencies. Each cross-section was evaluated in the range 10° x 10° around the selected orientation with 2° spacing over a regular grid. The arrows specify the directions of orientation change and their lengths indicate the corresponding magnitudes. The absence of arrows in the graphics corresponds to a negligible value of the calculated lattice-rotation rate. At this point, it is important to note that two points stand out in the construction of the lattice-rotation field map associated with a deformed state: i) when the Lagrangian approach is used to describe the texture evolution, orientations initially distributed following a regular grid do not maintain this regularity in the deformed state, ii) two orientations which are close in the deformed state may come from different initial orientations, which results from different deformation histories, consequently different accumulated shear, critical tensions, etc. can be found. To overcome these problems, we

added a fictitious set of orientations (i.e. their associated volume fractions are null) to the ensemble of orientations that described the material texture in order to evaluate the rotation field at these predefined grid positions. Furthermore, concerning the internal variables associated with these orientations − point charges −, it is necessary to assume they have the same microstructural state as the ideal orientation being investigated. In this sense, the calculated rotation-field map is not absolute. The starting orientations have to be specified in the analysis and their validity should be restricted to the vicinity of the orientation studied.

Lattice rotation field maps for the Cube and R-Cube orientations were calculated at the beginning of deformation and are displayed in Figure 3 and Figure 4, respectively.
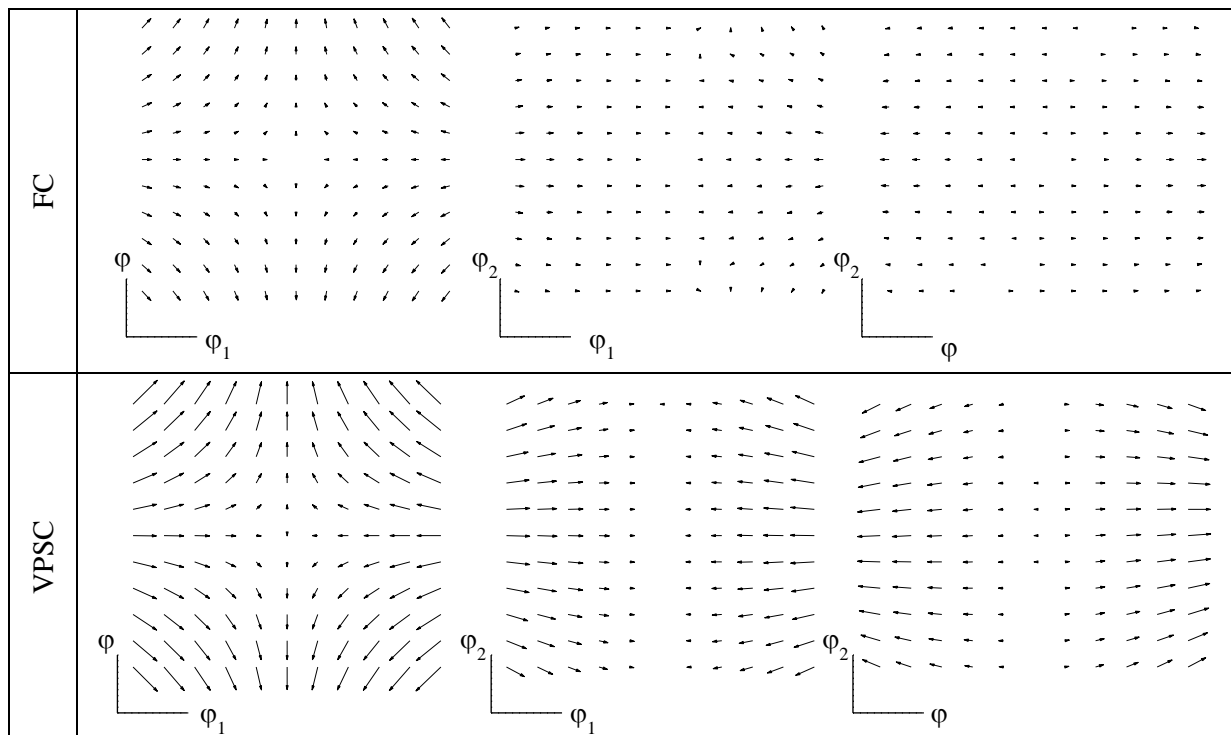
Figure 3: Lattice rotation fields map for the Cube orientation ($\varphi_1 = 0°$, $\phi = 90°$, $\varphi_2 = 90°$) predicted by the FC and VPSC models (multiplier magnitude 100).

It can be seen from Figure 3 that orientations around the ideal Cube behave symmetrically with respect to the axes for the three analyzed cross-sections. This characteristic is observed for both FC and VPSC models. The calculated rotation field converges on the φ_1 direction and diverges away from it in the ϕ direction, while a negligible rotation occurs along the φ_2 axis, particularly those orientations very close to the ideal Cube. Both schemes predict a flow of the rotation field that tends to move away in the direction of ϕ (i.e. towards the Goss orientations). Orientations rotate slowly during this process; however the predicted magnitudes of the lattice-rotation rates are stronger for the VPSC than for the FC model.

Shown in Table 2 and depicted in Figure 4, based on the rotation rates and the gradient values, results indicate that the R-Cube orientations are metastable. It can be seen in Figure 4 that, during plane strain deformation, a three-dimensional divergence is present in the rotation field around the ideal R-Cube. Results indicate that both schemes predict the same behavior; however, as shown for the Cube case, the magnitudes are more than two times larger for the VPSC calculations. As a consequence, a remarkable reduction in the intensity of this component occurs. The main lattice rotation takes place in the directions ϕ, φ_2, towards the Taylor orientation, and only a weak divergence is observed along the diagonal line; this can

be more easily seen in the $\varphi_2 - \phi$ section.
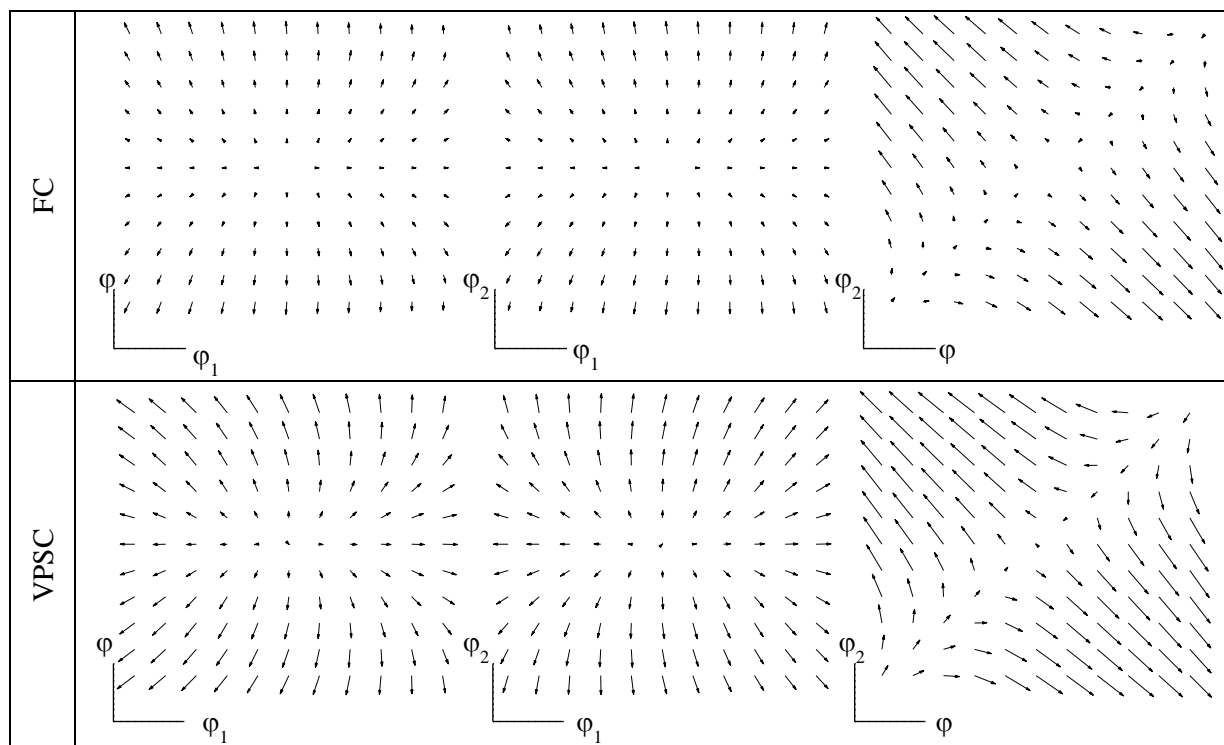
Figure 4: Rotation fields map for the R-Cube orientation ($\varphi_1 = 45°$, $\phi = 90°$, $\varphi_2 = 90°$) predicted by the FC and VPSC models (multiplier magnitude 50).

Figure 5 shows the initial and final (at limit-strain level) inverse pole figures for the Cube and R-Cube textured materials for plane-strain stretching. The inverse pole figures predicted at failure by both models are in close agreement with one other for the Cube material, but discrepancies between models take place for the R-Cube. As deformation proceeds, the initial R-Cube orientations move progressively to more stable positions S ($\varphi_1 = 59°$, $\phi = 37°$, $\varphi_2 = 63°$), Copper ($\varphi_1 = 90°$, $\phi = 35°$, $\varphi_2 = 45°$) and Taylor ($\varphi_1 = 90°$, $\phi = 27°$, $\varphi_2 = 45°$). The speed with which this happens makes the difference between the two models' predictions. At failure, VPSC has 75% of Copper and Taylor, 10% of S and no R-Cube orientations present, while the FC calculation retains an appreciable 20% of R-Cube and no Copper is reached.

The texture evolution during rolling of a polycrystalline aluminum alloy with initial Cube and R-Cube textures was experimentally investigated by Liu and Morris (2001, 2002). For the case of the initial Cube texture, the experimental results show that the Cube-oriented grains rotated to the β-fiber along different paths, leading to an increase of the intensity at the Copper and Taylor orientations. For the R-Cube texture, they found that grains with the {001}<110> orientation are unstable, and during rolling, they gradually rotate towards Copper and Taylor with a pronounced scattering towards S. As the cold-rolling reduction increases, the intensity of the R-Cube orientation decreases, while the intensity of orientations, shared by Copper and Taylor, increases. When the cold rolling reduction reaches about 64%, the intensity of R-Cube decreases to zero. VPSC predictions in plane strain are fully consistent with Liu and Morris' measurements.

Initial texture	Final texture	
	Cube	
	MK-FC	
	MK-VPSC	
	R-Cube	
	MK-FC	
	MK-VPSC	
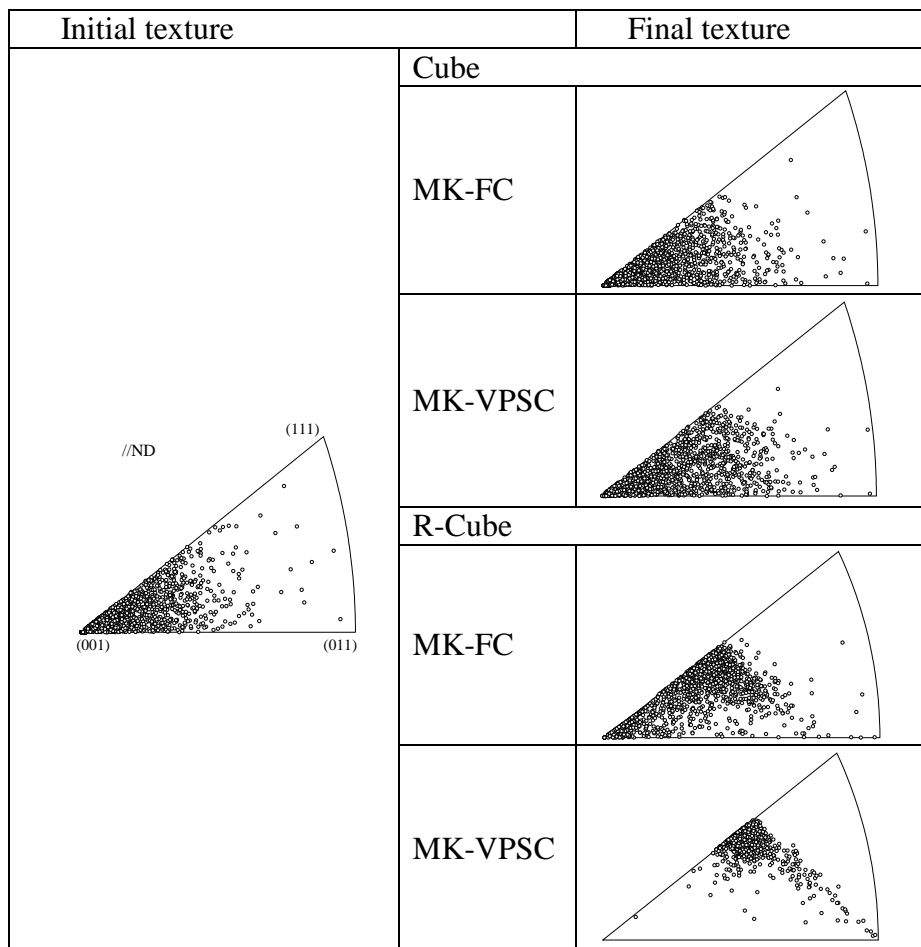
Figure 5: Equal-area inverse pole figures showing the initial (left) and predicted final (right) orientations at failure by MK-FC and MK-VPSC for the Cube and R-Cube textured materials.

Finally, in order to complete the present analysis, we plot the evolution of some of the ideal texture components during the deformation process; in particular we are interested in those orientations predicted at failure. Figure 6 shows the reorientation towards more stable positions of the initial Cube and R-Cube textured materials, for plain-strain stretching. Qualitatively, both models behave similarly for the main texture components, but differ in the velocity with which the process takes place, as was discussed previously. Tadano et al. (2012) recently highlighted similar results that show the relation between texture intensity and a sharper lattice rotation field for the case of a Cube-type texture treated within the FC or homogenization-based finite element method framework. The Cube texture shows the minor differences between both models in plain-strain loading (Figure 6 left), and it is interesting to note that the volume fraction of the cube orientations is around 35-40%. The main differences in magnitude appear for R-Cube (Figure 6 right). At the beginning of the deformation process, both FC and VPSC predict similar texture evolution, but as deformation proceeds quantitative and qualitative changes in the evolution profile are observed, in particular as the limit-strain values are approached. Near failure-strain, no R-Cube orientations are present in the VPSC simulated texture, while the FC calculation maintains nearly one third of the initial R-Cube orientations. A decomposition of the crystal orientations indicates that the reorientation towards the two complementary Copper-Taylor components is faster in VPSC than in FC calculations, and constitutes about 60% and 70% of the orientations at failure for both models, respectively. The same tendency is observed for the S orientations, but their intensities are

lower by an order of magnitude.
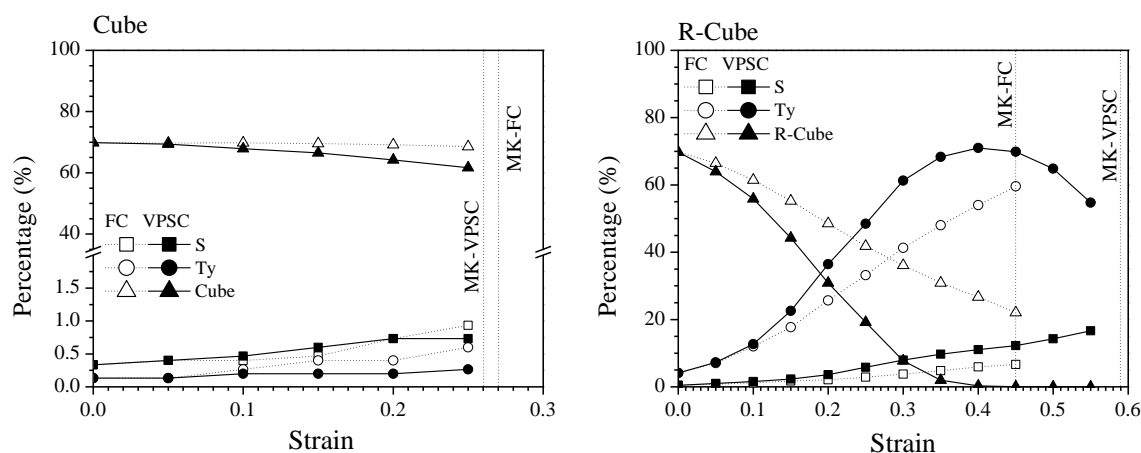
Figure 6: Evolution of the ideal texture-components in plain-strain and equi-biaxial stretching for Cube and R-Cube. The ideal components were calculated with a tolerance spread of 15 degrees.

So far, the orientational stability of Cube and R-Cube components in plane-strain have been evaluated and discussed in order to understand their evolution during plastic deformation. The final orientations depend on the selected model. This suggests that the way in which the initial textures evolve is the key to interpret the limit-strain profiles. In what follows, we present the correlation between orientation stability and the geometrical hardening due to grain rotations, as well as their effect on the predicted and enhanced forming-limit strains.

4 GEOMETRICAL HARDENING

Miller and Dawson, (1997) pointed out that the sources of the elevation of flow stress during straining can be delineated into material and geometric categories. The increase in the slip resistance, and hence of the macroscopic flow stress, as a result of dislocation interactions, is known as material hardening. Moreover, as plastic deformation proceeds, the grains rotate changing the orientations of each slip system. What results is an increase or decrease in the macroscopic flow stress required for continuous plastic deformation. This effect is referred to as geometrical (textural) hardening or softening. Yoshida et al. (2009) numerically investigated the geometrical hardening/softening effect for textured aluminum-alloy sheets in the plane-strain stretching mode using a generalized Taylor-type polycrystalline model. As they indicated, this effect appears to be effective in the development of high-formability sheet metal. To better understand whether the incorporation of the development of anisotropy during straining is at least as important as the effects of the initial grain distributions, we repeated the calculations of the limit-strain values but without texture evolution. Results, performed with both schemes for the plane-strain condition, are presented in Table 3. It should be noted that it is the texture evolution and not the particular initial texture considered here, which promotes high formability. When texture is not updated, the limit strains are all very close to each other, irrespective of the selected model.

	Cube		R-Cube	
	with	without	with	without
MK-FC	0.27	0.27	0.45	0.28
MK-VPSC	0.26	0.27	0.59	0.26

Table 3: Calculated limit-strain values, with and without texture evolution, at in plane-strain deformation around the Cube and R-Cube ideal orientations.

No effect is observed for the Cube texture, while it is evident that geometrical hardening takes place for the R-Cube case. Moreover, the greatest influence of geometrical hardening is predicted when the VPSC scheme is used, where the major limit strain is 1.3 times greater than for the FC calculation. The difference between models can be understood analyzing the geometrical stress/strain relations (i.e. calculations are carried out assuming that material hardening does not occur). The amount of strain nearly corresponds to the necking limit strains. The predicted stress-strain relations are displayed in Figure 7, where the macroscopic flow stress σ_{11} is normalized by $\sigma_{11(0)}$, which is the value of σ_{11} at $\varepsilon_{11} = 0$. The tendency reported in Yoshida's work is also observed with the VPSC scheme, but with a different strength. Thus, the importance of the polycrystal-plasticity scheme on the geometrical hardening, and therefore, on the FLD values can be clearly seen.
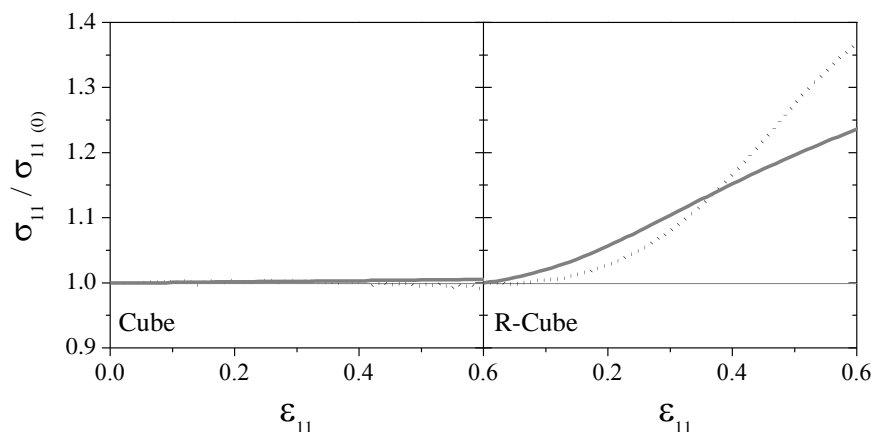
Figure 7: Normalized stress-strain curves in the plane-strain stretching mode.

As was shown in section 3, a very small amount of texture evolution is observed when the Cube texture is deformed, regardless of the model. At small deformations, $\varepsilon_{11} < 0.1$, grain rotations have a limited influence on the flow curve for R-Cube textures – using either FC or VPSC schemes –, but from this value the geometrical hardening has a non-negligible contribution. As deformation progresses, the differences between models are reflected in the slope of the plots. The velocity of change of geometrical hardening, and hence in the texture-evolution rate, are clearly illustrated. When the VPSC scheme is used, from approximately $\varepsilon_{11} = 0.25$ the R-Cube abruptly changes its slope and the geometrical hardening increases rapidly to its maximum value. On the other hand, when the FC scheme is used, the R-Cube texture exhibits only slightly differences between stages of hardening. The resulting flow curve is greater than for the VPSC model up to $\varepsilon_{11} = 0.38$, but from that point on the situation reverses and VPSC predicts a pronounced higher normalized flow stress. This response delays the occurrence of localized necking by a continuous positive change of the hardening rate, and therefore the limit strain values are higher in the VPSC simulations.

The lack of geometrical hardening predicted for the Cube orientation is consistent with the

calculated stability parameters, which are given in Table 1. The divergence is zero and almost null for FC and VPSC respectively, while the persistence value remains close to its maximum. As mentioned above, these orientations rotate slowly during plane-strain deformation; the rotation fields converge in one direction but diverge away from one another in the others. In contrast to the flow around Cube, significant geometrical hardening is observed around the R-Cube orientation. This fact is closely associated with the stability parameters calculated for the initial state of deformation. A three-dimensional divergence occurs, since all the gradients are positive, as shown in Table 2. Besides, the persistence parameters for both schemes are lower than those of Cube. The large differences in the predicted stability parameters are correlated with the different profiles displayed in Figure 7.

5 CONCLUSIONS

In the present study the role of the constitutive model in the forming limit of FCC sheet metal with Cube and R-Cube type material texture and stability analyses was investigated, confirming the relation between stability, geometrical hardening and the enhanced of formability close to plane-strain loading. Results show that the R-Cube orientations are metastable during rolling and, as deformation proceeds, rotate to Copper and Taylor orientations. The correlation between orientation stability and geometrical hardening was linked to the high formability in plane-strain loading. Texture evolution and the limit-strain predicted by VPSC are in agreement with experimental data reported by Liu et al. (2002) and Lopes et al. (2003) respectively.

REFERENCES

Arzhagui, M., Beausir, B., Tóth, L.,Contribution of non-octaedral slip to texture evolution of fcc polycrystals in simple shear. *Acta Materialia* 57: 2440–2453, 2009.

Beausir, B., Tóth, L., Neale, K.W., Ideal orientations and persistence characteristics of hexagonal close packed crystals in simple shear. *Acta Materialia* 55: 2695–2705, 2007.

Bertinetti, M.A., Turner, P.A., and Signorelli, J.W., Investigation of the effect of cube texture on formability of face center cubic sheet metals. *Mecánica Computacional Vol XXVII*, 899–907, 2008.

Choi, S.-H., Brem, J.C., Barlat, F., OH, K.H., Macroscopic anisotropy in AA5019A sheets. *Acta Materialia*, 48:1853–1863, 2000.

Clement, A., Coulomb, P., Eulerian simulation of deformation textures. *Scripta Metallurgica* 13:899–901, 1979.

Lopes, A.B., Barlat, F., Gracio, J.J., Ferreira Duarte, J.F., Rauch, E.F., Effect of texture and microstructure on strain hardening anisotropy for aluminum deformed in uniaxial tension and simple shear. *International Journal of Plasticity*, 19:1–22, 2003.

Liu, W.C., Man, C.-S., Morris, J.G., Lattice rotation of the cube orientation to the β fiber during cold rolling of AA 5052 aluminum alloy. *Scripta Materialia*, 45:807–814, 2001.

Liu WC, Morris JG. texture evolution of polycrystalline AA 5182 aluminum alloy with an initial {001}<110> texture during rolling. *Scripta Materialia*, 47:487–492, 2002.

Marciniak Z, Kuczynski K. Limit strains in the process of stretch-forming sheet metal. *International Journal of Mechanical Sciences* 9: 609–620, 1969.

Miller, M., Dawson, P., Influence of slip system hardening assumptions on modeling stress dependence of work hardening. *Journal of the* Mechanics *and Physics of Solids*, 45:1781–1804, 1997.

Pandey, A., Khan, A., Kim, E.-Y., Choi, S.-H., Gnäupel-Herold, T., Experimental and numerical investigations of yield surface, texture, and deformation mechanisms in AA5754

over low to high temperatures and strain rates. *International Journal of Plasticity*, 41:165−188, 2012.

Schwindt, C., Bertinetti, M.A., Signorelli, J.W., Influencia de estados de tensión de corte fuera del plano de la chapa en la curva límite de formabilidad. *Mecánica Computacional Vol XXXI*, 1767−1778, 2012.

Serenelli, M.J., Bertinetti, M.A., Signorelli, J.W., Study of limit strains for FCC and BCC sheet metal using polycrystal plasticity. *International Journal of Solids and Structures* 48:1109−1119, 2011.

Signorelli, J.W., Bertinetti, M,A., On the role of constitutive model in the forming limit of FCC sheet metal with cube orientations. *International Journal of Mechanical Sciences*, 51: 473−480, 2009.

Signorelli, J.W, Serenelli, M.J., Bertinetti, M,A., Experimental and numerical study of the role of crystallographic texture on the formability of an electro-galvanized steel sheet. *Journal Material Processing Technology*; 212:1367−1376, 2012.

Tadano, Y., Kuroda, M., Noguchi, H., Quantitative re-examination of Taylor model for FCC polycrystals. *Computational Material Science*, 51:290–302, 2012.

Tóth, L., Neale, K.W., Jonas, J.J., Stress response and persistence characteristics of the ideal orientations of shear textures. *Acta Metallurgica*, 37:2197–2210, 1989.

Wu, P.D., Mac Ewen, S.R., Lloyd, D.J., Neale, K.W., Effect of Cube Texture on Sheet Metal Formability. *Materials Science and Engineering* A, 364:182–187, 2004.

Yanaga, D., Kuwabara, T., Uema, N., Asano, M., Material modeling of 6000 series aluminum alloy sheets with different density cube textures and effect on the accuracy of finite element simulation. *International Journal of Solids and Structures*, 49:3488–3495, 2012.

Yoon, J.W., Barlat, F., Gracio, J.J., Rauch, E.F., Anisotropic strain hardening behavior in simple shear for cube textured aluminum alloy sheets. *International Journal of Plasticity*, 21:2426–2447, 2005.

Yoshida, K., Ishizaka, T., Kuroda, M., Ikawa, S., The Effects of Texture on Formability of Aluminum Alloy Sheets. *Acta Materialia*, 55:4499–4506, 2007.

Yoshida, K., Tadano, K., Kuroda, M., Improvement in formability of aluminum alloy sheet by enhancing geometrical hardening. *Computational Material Science*, 46:459–468, 2009.

Zhou, Y., Neale, K.W. Influence of f.c.c. rolling textures on biaxial sheet stretching. *Acta Metallurgica et Materialia*, 42: 2175–2189, 1994.